Unveiling electronic and magnetic properties of Cu3(SeO3)2Cl2 and Cu3(TeO3)2Br2 oxohalide systems via first-principles calculations

William Lafargue-Dit-Hauret, Xavier Rocquefelte

Unveiling electronic and magnetic properties of $Cu_3(SeO_3)_2Cl_2$ and $Cu_3(TeO_3)_2Br_2$ oxohalide systems via first-principles calculations

William Lafargue-Dit-Hauret

E-mail: william.lafargue-dit-hauret@univ-pau.fr
Univ Rennes, CNRS, ISCR (Institut des Sciences Chimiques de Rennes) UMR 6226, F-35000 Rennes, France

Xavier Rocquefelte

E-mail: xavier.rocquefelte@univ-rennes1.fr
Univ Rennes, CNRS, ISCR (Institut des Sciences Chimiques de Rennes) UMR 6226, F-35000 Rennes, France

September 2021

Abstract. Here, we report a theoretical investigation of the electronic and magnetic properties of two oxohalide compounds, namely $Cu_3(SeO_3)_2Cl_2$ and $Cu_3(TeO_3)_2Br_2$, using Density Functional Theory (DFT). These layered systems are characterized by two inequivalent Cu sites, with CuO_4 and CuO_4X (X = Cl, Br) environments, respectively. A new magnetic model is proposed through the calculation of the magnetic exchange couplings. Our study discloses the participation of the Se and Te lone-pairs to the long-range magnetic order, providing potential key informations for future chemical design of original magnetic systems.

Submitted to: *J. Phys.: Condens. Matter*

1. Introduction

Low-dimensional magnets and their exciting magnetic properties have fascinated both physicists and chemists for a long time. Great efforts have been devoted to synthesize such compounds which may exhibit exotic magnetic states such as spin-liquids, Bose-Einstein condensate, spin spirals or spin density waves [1, 2, 3, 4, 5]. These fundamental investigations notably enable the design of new low-dimensional magnetic networks through chemical routes, allowing to tune the topology of the magnetic centers (M) and their chemical environment (coordination, ligands). One strategy consists on using elements which have a stereochemically active electron pair [6]. An electron lone pair (usually noted E) is non-bonding and could replace a ligand in the coordination sphere of M, leading to a distorted chemical environment. For instance, the presence of structural channels in the compound $FeSb_2O_4$ is due to the pseudotetrahedral antimony site SbO_3E, i.e. three oxygen atoms and the lone pair of Sb(+III) [7].

Beyond the sterical effect on the atomic structure, these lone pairs may also participate actively to the electronic properties. Such a situation is typically observed in the ferroelectric compound $PbTiO_3$, which is known for its large polarization driven by the $6s^2$ electron lone pair of Pb(+II) [8, 9]. Indeed, the mechanism involves an off-centering of Pb atoms. A similar behaviour is observed with Bi(+III) in the well-known multiferroic compound $BiFeO_3$ [10].

Herein, we proposed a theoretical study of compounds which possess pseudotetrahedral entities based on $4s^2$ and $5s^2$ lone pairs of Se(+IV) and Te(+IV) species, respectively. These building blocks are encountered in a wide range of complex architectures [6, 11, 12, 13, 14, 15, 16, 17]. Two isostructural systems were chosen to rigorously compare the impact of the lone pair sites. Also, we took benefit of our experience in the modeling of Cu-based materials with *ab initio* approaches [18, 19, 20] to inspect the related magnetic properties of $Cu_3(SeO_3)_2Cl_2$ and $Cu_3(TeO_3)_2Br_2$ compounds [21, 22], abbreviated hereafter CSOC and CTOB, respectively. Magnetic susceptibility measurements on CTOB [23] evidenced a long range antiferromagnetic ordering below the Néel temperature, found at 67 K. The authors extracted the magnetic exchange coupling parameters from high temperature expansion analysis of the magnetic susceptibility, giving rise to a first magnetic model. However, such model does not allow to describe properly the magnetic properties below 150 K. In this study, we propose for the very first time theoretical insights for both CTOB and CSOC compounds to clarify the situation.

2. Computational details

First-principles calculations were performed using the Density Functional Theory (DFT) within the PAW method, as implemented in the Vienna Ab initio Simulation Package [24, 25, 26]. The Generalized Gradient Approximation defined by Perdew, Burke and Ernzerhof was considered for the exchange-correlation functional [27]. The overestimation of the intra-site electronic interactions for d-states is an intrinsic well-

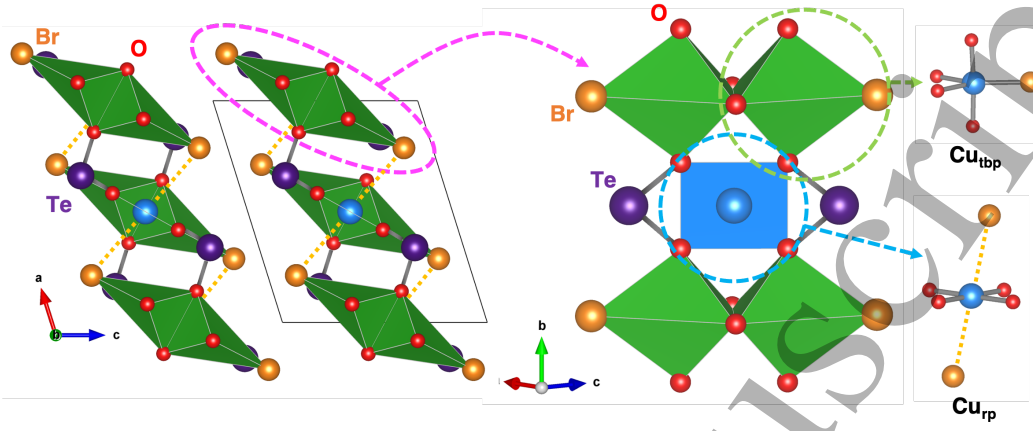

Figure 1. Crystal structure of $Cu_3(TeO_3)_2Br_2$ (CTOB). Cu, Te, O and Br atoms are indicated by blue, violet, red and orange spheres, respectively. Cu_{tbp} and Cu_{rp} environments are depicted by green and blue colors, respectively.

Table 1. Lattice cell parameters and number of formula units per unitcell for the CSOC and CTOB compounds.

Compounds	a (Å)	b (Å)	c (Å)	β (^{o})	Z
CSOC [22]	8.933	6.216	7.582	110.24	2
CTOB [21]	9.319	6.278	8.200	107.39	2

known problem of DFT. In this study, we corrected this error using the Hubbard approach with the rotationally invariant scheme [28]. According to this method, the on-site coulombic and exchange parameters, i.e. U and J respectively, need to be specified explicitly, which enables to recover the correct magnetic anisotropy [29]. Herein, we fixed $J = 0.8$ eV and varied the magnitude of U between 5 and 7 eV for the Cu $3d$ states, in the lines of previous investigations [30]. The planewave basis set was defined by a cut-off energy of 550 eV. The simulations were done using the experimental structures. The first Brillouin zones were investigated using the tetrahedron method corrected by Blöchl. Densities of States were determined using 8×10×9 and 7×10×8 Γ-centered k-meshes for CSOC and CTOB compounds, respectively.

3. Results and discussion

3.1. Description of the atomic structures

The isostructural CSOC and CTOB compounds crystallize in the monoclinic space group $C2/m$ (#12) [21, 22]. Their lattice parameters are reported in Table 1, and the unit cell of CTOB is depicted in Figure 1.

For both compounds, the atomic structure consists of layers stacked along the c axis and connected by van der Waals interactions. These layers are formed by chains made

Table 2. Electronic band gap (in eV) as a function of the U Hubbard parameter (J = 0.8 eV).

U	5 eV	6 eV	7 eV
CSOC	1.45	1.74	2.02
CTOB	1.38	1.67	1.97

up by Cu-based polyhedra and oriented along the [010] direction. Sellenite (SeO_3E) or tellurite (TeO_3E) groups link chains to each other. Two inequivalent crystallographic Cu sites are reported. One Cu atom (labelled Cu_{rp} hereafter) forms highly distorted CuO_4X_2 (X = Cl, Br) octahedra, with four oxygen atoms forming a rectangular planar environment (represented in blue in Figure 1), and two halogen atoms in apical positions, located at 3.09 Å and 3.34 Å from the Cu center, for Cl and Br, respectively. The second Cu atom (labelled Cu_{tbp} hereafter) forms a trigonal bipyramidal CuO_4X (X = Cl, Br) environment (shown in green in Figure 1), with two O and one halogen atoms in equatorial position and two O atoms in apical position. The two equatorial oxygen atoms are involved in edge-sharing connection between two Cu_{tbp} environments, while the two apical oxygen are involved in corner-sharing connection with a Cu_{rp} site.

3.2. Electronic properties

The calculated projected densities of states (pDOS) are shown in Figure 2 for CSOC and Figure 3 for CTOB, with U = 6 eV and J = 0.8 eV. The electronic ground state is found to be insulating for both compounds, with a band gap of 1.74 and 1.67 eV for CSOC and CTOB, respectively. The valence band, from -8 to 0 eV, is composed by O $2p$ and halogen p states, which strongly hybridize with the Cu $3d$ states. The interaction between Se (Te) and O atoms only appears in the lower part of the valence bands, i.e. below -4 eV. Such analysis emphasizes that the chemical substitution of Se by Te species and Cl by Br atoms does not significantly alter the electronic properties.

The DOS of the two inequivalent Cu sites are significantly different. Indeed, while the sum of the d_{xy}, d_{xz}, d_{yz} and d_{z^2} contributions has more or less the same DOS shape, $d_{x^2-y^2}$ orbital allows to distinguish both sites. For Cu_{rp}, the related electronic states are strongly localized in the lower part of the valence band and around 2 eV above the Fermi energy. Within the same energy range, the Cu_{tbp} $d_{x^2-y^2}$ band is broader. The increase of the U Hubbard parameter reduces the dispersion of Cu $3d$ states and increases the splitting of up and down states, leading to larger band gap values as reported in Table 2.

To go deeper into the analysis, we calculated the electronic bandstructures (see Figure 4 for the CSOC compound). As expected from the results discussed above, similar behaviors are observed for both compounds. The electronic band gap is slightly indirect, the top of the valence bands being located at the C point, while the bottom

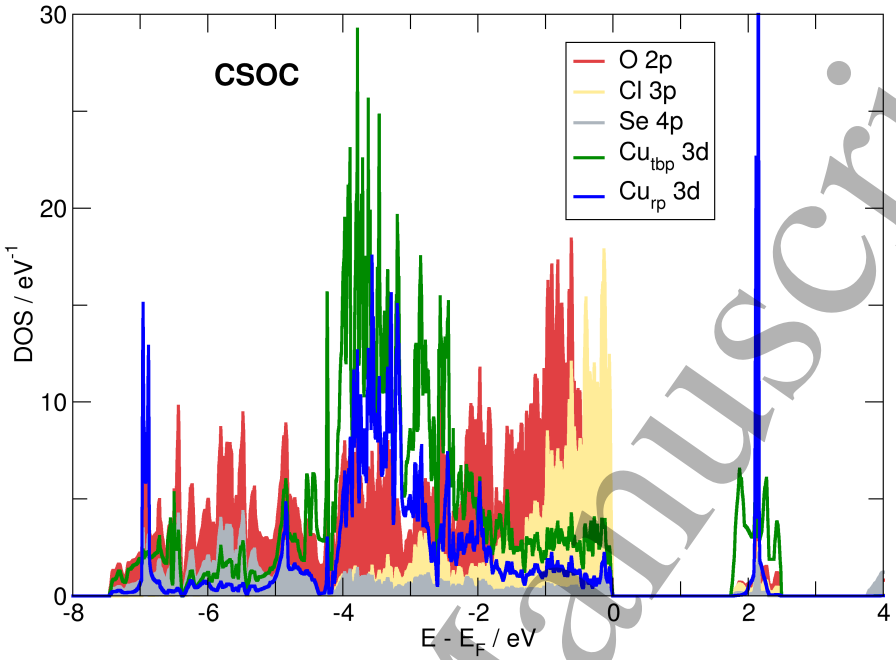

Figure 2. Projected densities of states of CSOC on Cu $3d$, Se $4p$, O $2p$ and Cl $3p$ orbitals. Results were obtained with $U = 6$ eV and $J = 0.8$ eV. The Fermi energy is set to zero.

of the conduction bands appears at the E point. Between -4 and -8 eV, the dispersive bands show strong Se and O characters, which are attributed to the sellenite groups. As observed in the pDOS, Cu_{rp} $d_{x^2-y^2}$ states are strongly localized, while Cu_{tbp} interact with the SeO_3E environment. This observation evidences that the Cu_{tbp} environments are more sensitive to the Se/Te substitution than Cu_{rp} sites. At the upper part of the valence band, the O $2p$ and halogen p states are more localized. Regarding the lower part of the conduction band, we retrieve the strong localization of Cu_{rp} $d_{x^2-y^2}$ states just above 2 eV, while Cu_{tbp} $d_{x^2-y^2}$ states are dispersed along the $[010]^*$ direction. In the real space, it corresponds to the [010] crystallographic direction along which the chains are oriented. This dispersion is the fingerprint of stronger covalent interactions within the chain involving edge-sharing Cu_{tbp} environments.

3.3. Collinear magnetic properties

Herein, we detailed the investigation of magnetic exchange interactions between Cu atoms. A first attempt to explain the entire magnetic phase diagram of CTOB has been done by Uematsu *et al* [23]. Based on high temperature expansion analysis of the magnetic susceptibility, two magnetic interactions within a chain have been determined: i) an antiferromagnetic (AFM) coupling of 24.1 meV between Cu_{rp} and Cu_{tbp} sites, and

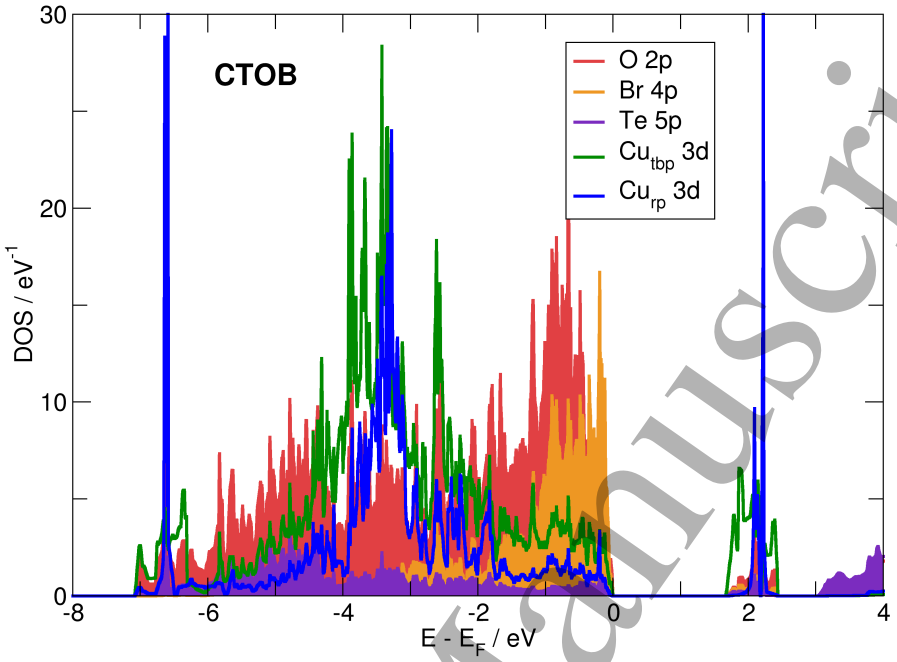

Figure 3. Projected densities of states of CTOB on Cu 3*d*, Te 5*p*, O 2*p* and Br 4*p* orbitals. Results were obtained with $U = 6$ eV and $J = 0.8$ eV. The Fermi energy is set to zero.

ii) a ferromagnetic (FM) coupling of -2.0 meV between two neighboring Cu_{tbp} centers. Because this model fails to describe the magnetic susceptibility below 150 K, they proposed to add an effective inter-chain coupling. Here, we propose to shed light on these microscopic mechanisms using *ab initio* methods.

The six magnetic interactions considered in this study are depicted in Figure 5a. Two of them consist of intra-chain superexchange (SE) interactions, i.e. J_{ch} and J_d, corresponding to the ones already reported. Four inter-chain super-superexchange (SSE) couplings J_i are considered here, involving the electron lone pair E of Se and Te atoms. The corresponding experimental Cu-Cu distances are reported in Table 3 for CSOC and Table 4 for CTOB.

The J exchange interactions were estimated based on the experimental structures, and varying the U Hubbard term. We calculated the total energy of 13 collinear spin orderings defined in a 2×1×1 supercell. 2×8×7 and 2×8×6 Γ-centered k-meshes were used for the first Brillouin zone sampling of CSOC and CTOB, respectively. An Ising Hamiltonian was used to map the DFT energies through a least-squares fit procedure. For a given m collinear magnetic order, the energy of the Ising model is expressed as:

$$E^m_{Ising} = \alpha^m_{ch} J_{ch} S_{rp} \cdot S_{tbp} + \alpha^m_d J_d S_{tbp} \cdot S_{tbp} + \alpha^m_{i1} J_{i1} S_{rp} \cdot S_{tbp}$$

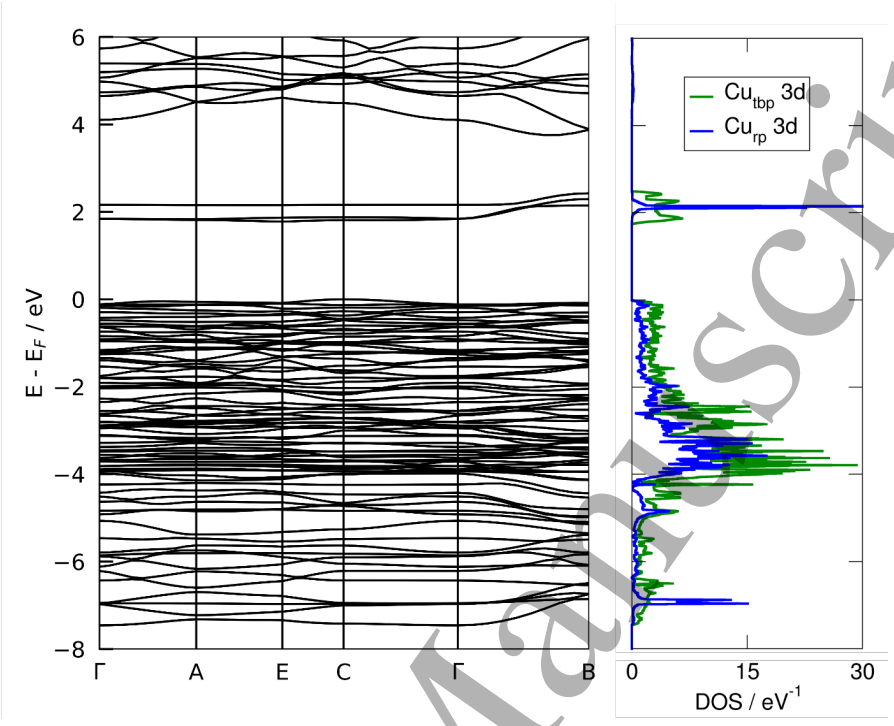

Figure 4. Bandstructure of CSOC with the pDOS of Cu_{rp} 3d and Cu_{tbp} 3d. Results were obtained with $U = 6$ eV and $J = 0.8$ eV. The Fermi energy is set to zero.

$$+ \alpha^m_{i2} J_{i2} S_{tbp} \cdot S_{tbp} + \alpha^m_{i3} J_{i3} S_{tbp} \cdot S_{tbp} + \alpha^m_{i4} J_{i4} S_{rp} \cdot S_{tbp} \quad (1)$$

where α^m_j is the coefficient associated to the J_j exchange coupling between two spins. S_{rp} and S_{tbp} correspond to the spins carried by the Cu_{rp} and Cu_{tbp} atoms, respectively. The estimated J exchange couplings are reported for each U values in Tables 3 and 4 for CSOC and CTOB, respectively. The deviation for each magnetic state between DFT (with $U = 6$ eV) and the Ising model is shown for CTOB in Figure 5b.

3.4. Magnetic ground state

The comparison between the DFT energies of the different collinear magnetic orders reveals that the most unstable state is the FM state, while the most stable one corresponds to an AFM structure, in agreement with the experimental data reporting a low-temperature AFM ordering. Considering the most stable AFM state with $U = 6$ eV and $J = 0.8$ eV, the local magnetic moments of Cu_{rp} and Cu_{tbp} for both compounds are close to 0.7 μ_B, as expected for Cu^{2+} ions. The equatorial O, Cl and Br atoms of the Cu_{tbp} environment carry relatively small magnetic moments (smaller than 0.06 μ_B), while the other atoms show non-significant values. The two most stable AFM states, labelled AFM_1 and AFM_2 hereafter, are depicted in Figure 6. Within a chain, both of them are characterized by an AFM alignment of Cu_{rp} and Cu_{tbp} spins, and a FM alignment of neighboring Cu_{tbp} spins. In the most stable AFM ordering, i.e. the

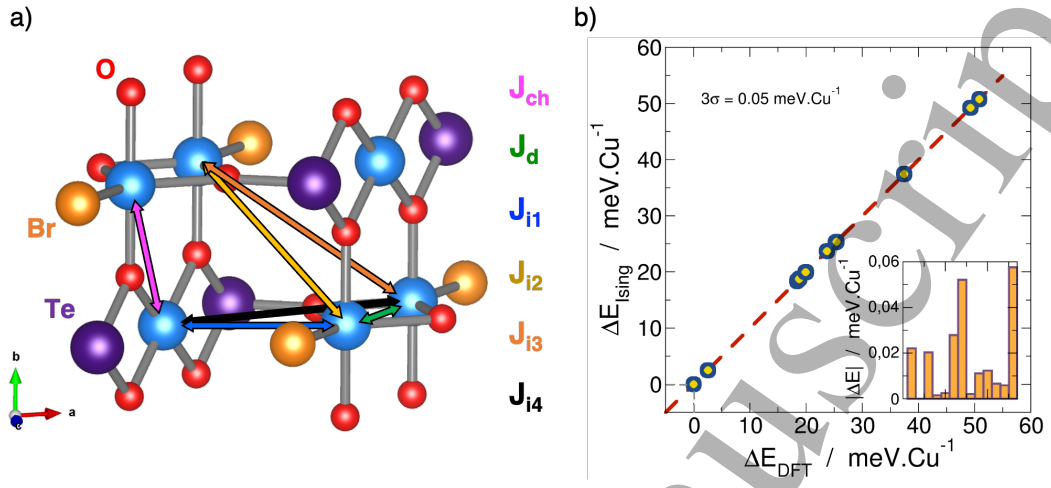

Figure 5. a) Magnetic exchange interactions which are considered in this work for both compounds. Cu atoms are evidenced with cyan color. Violet and orange spheres indicate Te (Se) and Br (Cl) atoms, respectively, while red spheres indicate O atoms. b) Relative energies of CTOB with 13 inequivalent collinear magnetic configurations predicted by the Ising model versus the relative DFT energies. The dashed line evidences the perfect agreement between the Ising Hamiltonian and DFT calculations. The inset shows the deviation between the values of the model and those from DFT for each magnetic configuration.

AFM_1 state, the Cu_{rp} and Cu_{tbp} spins belonging to two different chains are FM coupled, while they are AFM coupled in the AFM_2 state. It confirms the importance to properly estimate the inter-chain couplings to distinguish the two magnetic states and access low-temperature magnetic properties.

Figure 7 shows the spin densities of the magnetic ground state, i.e. the AFM_1 state, for both compounds. The magnetically active orbital, i.e. $d_{x^2-y^2}$, clearly appears, as expected from the d^9 electronic configuration of Cu_{rp} and Cu_{tbp}. The analysis of the spin densities highlights the magnetic exchange paths, which are driven by the orbital overlaps. Here, the opposite sign of spin densities between neighboring Cu_{rp} and Cu_{tbp} sites lets suggest an AFM J_{ch} coupling, while a FM interaction is expected between neighboring Cu_{tbp} centers, in the lines of the previously established magnetic model [23]. We also noticed that more spin density is carried by Cl than Br atoms. A slightly larger electronegativity and smaller ionic size for Cl than Br would probably favor the spread of the magnetism carried by neighboring Cu_{tbp} sites in the case of CSOC.

3.5. Magnetic exchange couplings

The calculated magnetic exchange couplings are reported for each U values in Table 3 and Table 4 for CSOC and CTOB, respectively. For $U = 6$ eV, the J_{ch} coupling between Cu_{rp} and Cu_{tbp} sites is found to be strongly AFM in CSOC (79.4 meV) and CTOB (73.1 meV), explaining the AFM ground state. In contrast to previous expectations [23], J_d is

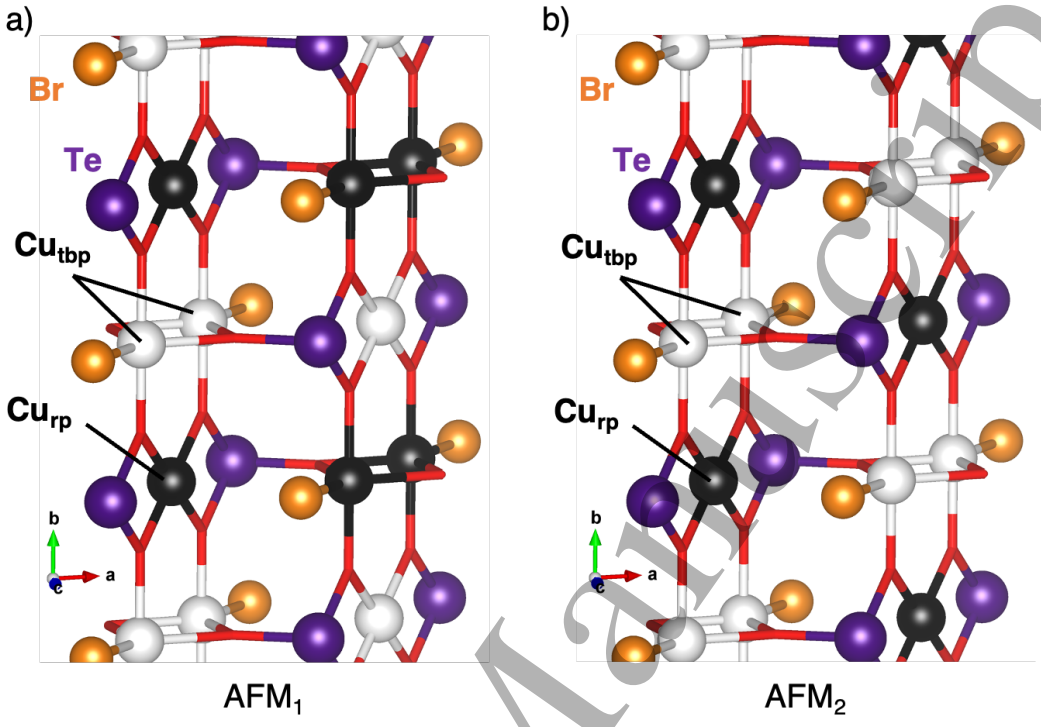

Figure 6. Comparison of a) the most stable (labelled AFM_1) and b) the second most stable (labelled AFM_2) collinear magnetic states. The up- and down-spins Cu^{2+} sites are indicated by black and white spheres, respectively. O atoms are removed for clarity.

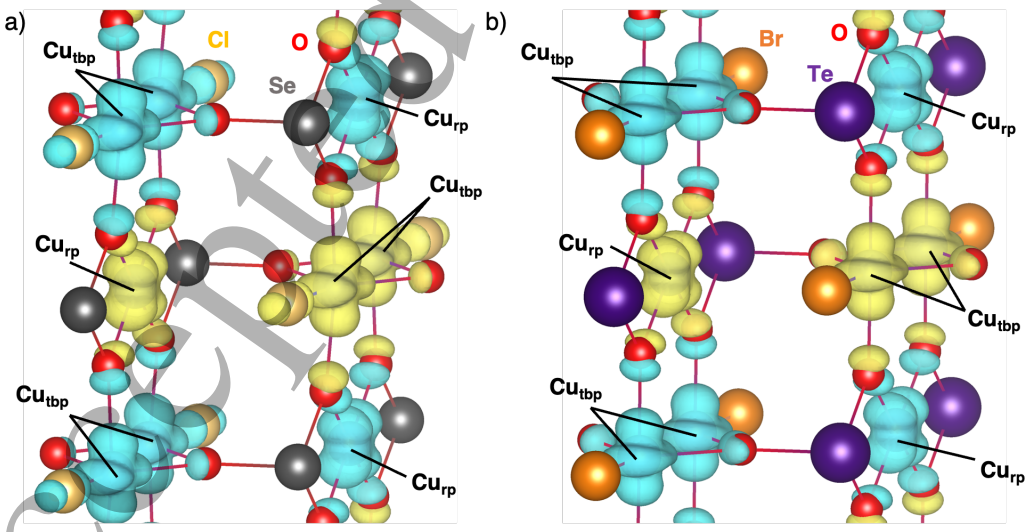

Figure 7. Spin densities of the magnetic ground state of a) CSOC and b) CTOB compounds. Cu and O atoms are indicated by cyan and red spheres, respectively. Black (violet) and gold (orange) spheres indicate Se (Te) and Cl (Br) atoms. Cyan and yellow shapes evidence up and down spin-densities, respectively.

Table 3. Magnetic exchange couplings (in meV) of the CSOC compound varying the U parameter from 5 to 7 eV ($J = 0.8$ eV). $J > 0$ and $J < 0$ indicate AFM and FM interactions, respectively.

Couplings	J_{ch}	J_d	J_{i1}	J_{i2}	J_{i3}	J_{i4}
d_{Cu-Cu} (Å)	3.534	3.363	3.607	4.625	5.442	5.705
$U = 5$ eV	95.6	9.9	-0.4	2.3	0.0	-1.3
$U = 6$ eV	79.4	5.3	-0.3	1.9	0.1	-1.0
$U = 7$ eV	65.3	2.7	-0.3	1.5	0.1	-0.9

Table 4. Magnetic exchange couplings (in meV) of the CTOB compound varying the U parameter from 5 to 7 eV ($J = 0.8$ eV). Results from the high temperature expansion done by Uematsu *et al* [23] is added for the comparison. $J > 0$ and $J < 0$ indicate AFM and FM interactions, respectively.

Couplings	J_{ch}	J_d	J_{i1}	J_{i2}	J_{i3}	J_{i4}
d_{Cu-Cu} (Å)	3.511	3.145	3.709	4.539	5.618	5.883
$U = 5$ eV	87.8	9.0	-0.6	8.0	-0.1	-1.1
$U = 6$ eV	73.1	4.5	-0.7	6.6	-0.2	-0.7
$U = 7$ eV	60.2	3.0	-0.3	4.8	0.0	-0.9
HTE [23]	24.1	-2.0	-	-	-	-

predicted to be AFM in CSOC (4.5 meV) and CTOB (5.3 meV). Concerning the inter-chain couplings, we estimated the AFM J_{i2} interaction at 1.9 and 6.6 eV for CSOC and CTOB, respectively, while J_{i1}, J_{i3} and J_{i4} appear negligible. A similar general trend is observed with the other U values, where the overall of J exchange couplings tends to increase with the decrease of the U parameter.

The comparison between the two compounds allows to emphasize the strong influence of sellenite (SeO_3E) and tellurite (TeO_3E) groups on the J_{ij} interactions. For example, the substitution of Se by Te nearby the $Cu_{rp}O_4$ environment increases the O-Cu_{rp}-O angle from 75.2 to 78.7°. While the Cu_{rp}-O-Cu_{tbp} angle and the distance between magnetic centers remain similar, the O-Cu_{rp}-O distortion is probably at the origin of higher values for the J_{ch} intra-chain coupling in CSOC. Moreover, the presence of SeO_3E groups significantly distort the atomic structure of CSOC compared to the CTOB one. Such a situation results from the combination of a large inter-chain O-Se-O angle (102.8°) and short Se-O bond lengths (1.663 Å-1.738 Å) induced by the lone pair E, while TeO_3E groups show a smaller inter-chain O-Te-O angle (99.3°) and longer Te-O bond lengths (1.835 Å-1.909Å). For the CSOC compound, these structural distortions induces an asymmetry in Cu_{tbp}-O-Cu_{tbp} path which weakens the J_{i2}. In the case of J_d, such distortions could compensate the increase of the d_{Cu-Cu} distance compared to CTOB, as evidenced by a rather similar value for the magnetic interaction.

Here, we showed that the increase of the U parameter from 5 to 7 eV reduces the strength of J_{ch} from 87.8 to 60.2 meV. In their study, Uematsu *et al* reported a three times lower value for this coupling, being estimated at 24.1 meV [23]. Also, the authors explained the FM alignment of neighboring Cu_{tbp} spins by a FM coupling, following the chemical intuition dictated by the Kanamori-Goodenough-Anderson rules. Our simulations evidence the situation could be more complex than expected. We found that the FM effective ordering is indeed a consequence of the combination of two AFM couplings, i.e. J_{ch} and J_d. Finally, the inter-chain AFM J_{i2} interaction is non-negligible and favors the stabilization of the AFM_1 ground state compared to the AFM_2 state. If such inter-chain interaction has already been evoked before [23], our study reveals for the first time its importance.

4. Conclusions

We reported the theoretical study of the electronic and magnetic properties of the $Cu_3(SeO_3)_2Cl_2$ and $Cu_3(TeO_3)_2Br_2$ compounds, based on their experimental structures. Both structures possesses two inequivalent crystallographic Cu^{2+} sites with CuO_4 and CuO_4X (X = Cl, Br) environments. Our DFT calculations revealed the electronic signature of each Cu^{2+} site. The study of the magnetic exchange couplings allows us to propose a ground state magnetic model for these two compounds. We evidenced that i) the FM alignment of neighboring Cu_{tbp} spins is the result of two AFM couplings, and ii) an inter-chain AFM interaction is responsible for a FM inter-chain alignment.

Acknowledgments

We thank access to the HPC resources of [TGCC/CINES/IDRIS] under allocation 2017-A0010907682 made by GENCI, and CCIPL (Centre de Calcul Intensif des Pays de la Loire) for computing facilities. Crystal structures were represented using the VESTA software [31].

References

[1] Fawcett E 1988 *Reviews of Modern Physics* **60** 209–283 URL https://link.aps.org/doi/10.1103/RevModPhys.60.209

[2] Kimura T, Sekio Y, Nakamura H, Siegrist T and Ramirez A P 2008 *Nature Materials* **7** 291–294 ISSN 14761122 URL http://search.ebscohost.com/login.aspx?direct=true&db=a9h&AN=31343383&lang=fr&site=ehost-live

[3] Dutton S E, Kumar M, Mourigal M, Soos Z G, Wen J J, Broholm C L, Andersen N H, Huang Q, Zbiri M, Toft-Petersen R and Cava R J 2012 *Physical Review Letters* **108** 187206 URL https://link.aps.org/doi/10.1103/PhysRevLett.108.187206

[4] Zapf V 2014 *Rev. Mod. Phys.* **86** 563–614

[5] Fu M, Imai T, Han T H and Lee Y S 2015 *Science* **350** 655–658 ISSN 0036-8075, 1095-9203 URL https://science.sciencemag.org/content/350/6261/655

[6] Berdonosov P S, Kuznetsova E S and Dolgikh V A 2018 *Crystals* **8** 159 URL https://www.mdpi.com/2073-4352/8/4/159

[7] de Laune B P, Rees G J, Whitaker M J, Hah H Y, Johnson C E, Johnson J A, Brown D E, Tucker M G, Hansen T C, Berry F J, Hanna J V and Greaves C 2017 *Inorganic Chemistry* **56** 594–607 ISSN 0020-1669 URL https://doi.org/10.1021/acs.inorgchem.6b02466

[8] Cohen R E 1992 *Nature* **358** 136–138 ISSN 1476-4687 URL https://www.nature.com/articles/358136a0

[9] Kuroiwa Y, Aoyagi S, Sawada A, Harada J, Nishibori E, Takata M and Sakata M 2001 *Physical Review Letters* **87** 217601 URL https://link.aps.org/doi/10.1103/PhysRevLett.87.217601

[10] Ravindran P, Vidya R, Kjekshus A, Fjellvåg H and Eriksson O 2006 *Physical Review B* **74** 224412 URL https://link.aps.org/doi/10.1103/PhysRevB.74.224412

[11] Kahn O, Verdaguer M, Girerd J J, Galy J and Maury F 1980 *Solid State Communications* **34** 971–975 ISSN 0038-1098 URL http://www.sciencedirect.com/science/article/pii/0038109880911102

[12] Johnsson M, Törnroos K W, Lemmens P and Millet P 2003 *Chemistry of Materials* **15** 68–73 ISSN 0897-4756 URL https://doi.org/10.1021/cm0206587

[13] Takagi R, Johnsson M, Kremer R K and Lemmens P 2006 *Journal of Solid State Chemistry* **179** 3763–3767 ISSN 0022-4596 URL http://www.sciencedirect.com/science/article/pii/S0022459606004658

[14] Bos J W G, Colin C V and Palstra T T M 2008 *Physical Review B* **78** 094416 URL https://link.aps.org/doi/10.1103/PhysRevB.78.094416

[15] Kovrugin V M, Colmont M, Mentré O, Siidra O I and Krivovichev S V 2016 *Mineralogical Magazine* **80** 227–238 ISSN 0026-461X, 1471-8022 URL https://www.cambridge.org/core/journals/mineralogical-magazine/article/dimers-of-oxocentred-ocu46-tetrahedra-in-two-novel-copper-selenite-chlorides-kcu3oseo32cl-and-na2C13FE8606D4669F6B50034BEBC11CFB

[16] Wu H C, Chandrasekhar K D, Yuan J K, Huang J R, Lin J Y, Berger H and Yang H D 2017 *Physical Review B* **95** 125121 URL https://link.aps.org/doi/10.1103/PhysRevB.95.125121

[17] Hu S and Johnsson M 2012 *Dalton Transactions* **41** 12786–12789 ISSN 1477-9234 URL https://pubs.rsc.org/en/content/articlelanding/2012/dt/c2dt31188g

[18] Kenney E M, Segre C U, Lafargue-Dit-Hauret W, Lebedev O I, Abramchuk M, Berlie A, Cottrell S P, Simutis G, Bahrami F, Mordvinova N E, Fabbris G, McChesney J L, Haskel D, Rocquefelte X, Graf M J and Tafti F 2019 *Physical Review B* **100** ISSN 2469-9950, 2469-9969 URL https://link.aps.org/doi/10.1103/PhysRevB.100.094418

[19] Novosel N, Lafargue-Dit-Hauret W, Rapljenović v, Dragičević M, Berger H, Cinčić D, Rocquefelte X and Herak M 2019 *Phys. Rev. B* **99** 014434 URL https://link.aps.org/doi/10.1103/PhysRevB.99.014434

[20] Lafargue-Dit-Hauret W, Braithwaite D, Huxley A D, Kimura T, Saúl A and Rocquefelte X 2021 *Physical Review B* **103** 214432 URL https://link.aps.org/doi/10.1103/PhysRevB.103.214432

[21] Becker R, Johnsson M, Kremer R K and Lemmens P 2005 *Journal of Solid State Chemistry* **178** 2024–2029 ISSN 0022-4596 URL http://www.sciencedirect.com/science/article/pii/S0022459605001520

[22] Becker R, Berger H and Johnsson M 2007 *Acta Cryst C, Acta Cryst Sect C, Acta Crystallogr C, Acta Crystallogr Sect C, Acta Crystallogr C Cryst Struct Commun, Acta Crystallogr Sect C Cryst Struct Commun* **63** i4–i6 ISSN 0108-2701 URL http://scripts.iucr.org/cgi-bin/paper?bc3024

[23] Uematsu D and Sato M 2007 *J. Phys. Soc. Jpn.* **76** 084712 ISSN 0031-9015 URL https://journals.jps.jp/doi/abs/10.1143/JPSJ.76.084712

[24] Kresse G and Furthmüller J 1996 *Computational Materials Science* **6** 15–50 ISSN 0927-0256 URL http://www.sciencedirect.com/science/article/pii/0927025696000080

[25] Kresse G and Furthmüller J 1996 *Phys. Rev. B* **54** 11169–11186 URL http://link.aps.org/

doi/10.1103/PhysRevB.54.11169

[26] Kresse G and Joubert D 1999 *Phys. Rev. B* **59** 1758–1775 URL http://link.aps.org/doi/10.1103/PhysRevB.59.1758

[27] Perdew J P, Burke K and Ernzerhof M 1996 *Phys. Rev. Lett.* **77** 3865–3868 URL https://link.aps.org/doi/10.1103/PhysRevLett.77.3865

[28] Liechtenstein A I, Anisimov V I and Zaanen J 1995 *Phys. Rev. B* **52** R5467–R5470 URL http://link.aps.org/doi/10.1103/PhysRevB.52.R5467

[29] Bousquet E and Spaldin N 2010 *Phys. Rev. B* **82** 220402 URL http://link.aps.org/doi/10.1103/PhysRevB.82.220402

[30] Lee C, Liu J, Whangbo M H, Koo H J, Kremer R K and Simon A 2012 *Phys. Rev. B* **86** 060407 URL https://link.aps.org/doi/10.1103/PhysRevB.86.060407

[31] Momma K and Izumi F 2011 *Journal of Applied Crystallography* **44** 1272–1276 ISSN 0021-8898 URL http://scripts.iucr.org/cgi-bin/paper?db5098